ELSEVIER

Journal of Nuclear Materials 320 (2003) 223–230

journal of nuclear materials

www.elsevier.com/locate/jnucmat

Application of hydrogen analysis by neutron imaging plate method to Zircaloy cladding tubes

Ryou Yasuda [a,*], Masahito Nakata [a], Masahito Matsubayashi [b], Katsuya Harada [a], Yuichi Hatakeyama [a], Hidetoshi Amano [a]

[a] *Department of Hot Laboratories, Japan Atomic Energy Research Institute, Tokai-mura, Naka-gun, Ibaraki-ken 319-1195, Japan*

[b] *Japan Atomic Energy Research Institute, Center for Proton Accelerator Facilities, Tokai-mura, Naka-gun, Ibaraki-ken 319-1195, Japan*

Received 24 March 2002; accepted 24 February 2003

Abstract

Effectiveness of neutron imaging plate (NIP) method for hydrogen analysis is investigated by using standard samples with known hydrogen concentrations. A relationship between hydrogen concentration in Zircaloy tubes and numerical data in the NIP images was obtained by image analysis process. By using the relationship, local hydrogen concentrations in segregated tubes with heterogeneous hydrogen distribution were estimated in a small area; 0.1×0.1 mm^2. Contribution of an oxide film in the tubes to the images is also investigated by using oxidized samples with and without hydrides. In the NIP images of the oxidized samples, oxide film was not recognized in the images of the sample. Results of numerical analysis also show no effect of the oxide film. These results show that the effect of oxygen in the image can be neglected when hydrogen analysis is performed on the Zircaloy tube with oxide film and hydrides by NIP method.

PACS: 28.52.Fa; 29.30.Hs; 28.50.Dr

1. Introduction

It is well-known that the absorbed hydrogen into Zircaloy tubes is generated with formation of oxide films under a light water reactor environment. The reaction formula is shown by

$$Zr + 2H_2O \rightarrow ZrO_2 + 4H \quad (1)$$

Embrittlement of the cladding tubes caused by the absorbed hydrogen is regarded as one of the important issues from the safety viewpoint of the extended burn-up fuels [1–3]. In the pellet–cladding mechanical interaction induced with the reactivity induced accidents on high burn-up fuels, it is considered that highly concentrated hydrogen accelerates failure of the Zircaloy tubes. Knowledge of distribution of hydrogen concentration in the irradiated cladding tube is hence significant to evaluate its safety and reliability.

High temperature extraction method and metallographic observation of an acid-etched sample have been representative hydrogen analyses in the post irradiation examinations. High temperature extraction method has good accuracy in measuring hydrogen concentration in solid materials. However, the samples for the method are melted during examination, becoming unusable for further examinations and analyses. Although metallographic observation is effective to evaluate the hydrogen distribution qualitatively, quantitative estimation of the hydrogen concentration is limited. The quantitative relationship between the etched area and hydrogen concentrations is actually unclear.

* Corresponding author. Tel.: +81-29 282 5727; fax: +81-29 282 5923.

E-mail address: yasuda@dhl.tokai.jaeri.go.jp (R. Yasuda).

0022-3115/03/$ - see front matter
doi:10.1016/S0022-3115(03)00112-0

Neutron radiography has been used as an effective tool for viewing the hydrogen distribution in Zircaloy tubes, because the scattering cross-section of hydrogen for a thermal neutron is larger than that of Zr–matrix atom [4–6]. Advanced neutron radiography techniques including the neutron imaging plate (NIP) were developed in the last decade [7]. The high sensitivity and wide dynamic range of NIP make it possible to shorten the exposure time, to perform quantitative evaluation, and to display images without complicated film development processes.

In the previous work, the effectiveness of NIP and the neutron computed tomography (NCT) methods for estimating hydrogen concentration and its distribution in unirradiated Zircaloy cladding tubes with hydrides were investigated [8]. The hydrides were segregated at circumference region in the tubes to imitate irradiated cladding tubes in the pressurized water reactor (PWR). The hydrided region was confirmed in the images of NIP and NCT. A relationship between the average hydrogen concentration over the samples and the numerical data in the images was also found. However, the relationship was not suitable to use for calibration of numerical data in the image to the hydrogen concentration directly, because hydrogen distribution in the samples was hence inhomogeneous. The local hydrogen concentration in the samples has not been known, yet.

Contribution of oxide films in Zircaloy tubes to the images has not also been investigated, yet. Absorption of hydrogen into the tube follows the formation of the oxide film as shown by Eq. (1). Distinction between the regions of the hydride and oxide film in the image is required to estimate hydrogen concentrations by NIP images, because the oxide film is formed at the outer surface in the irradiated tubes; i.e., at the outer vicinity of the hydrided region. It is hence significant to know the contribution of the oxide film to the images from the viewpoint of application of NIP method to hydrogen analysis.

In this paper, the following investigated subjects are described: (1) more suitable relationship between hydrogen concentration in Zircaloy tubes and numerical data in the images using 'standard samples' with controlled amount of hydrogen concentrations and (2) influence of the oxide film in the tubes on the NIP images is also investigated by comparing the images of the hydrided samples to those of the oxidized samples with and without the hydrides. The contribution of the oxide film to the hydrogen analysis by NIP method is also discussed.

2. Experimental

2.1. Examinations

Zircaloy-2 tubes with oxide film were used in the examinations. The thickness and outer diameter of the Zircaloy-2 tubes were 0.82 and 14.5 mm, respectively. The chemical composition of the used samples satisfies the ASTM Standard, B351-85 [9]. Oxide films with controlled thicknesses of around 30 and 70 μm, were formed on the inner and outer surfaces under steam gas flow at 973 and 1323 K, respectively. Samples 5 mm in length were cut from those tubes. It is noted that the Zircaloy-2 tube processed at 1323 K contained α-phase region around 80 μm in width in the inner vicinity of the oxide film. The α-phase contained much dissolute-oxygen in the matrix. Highly concentrated oxygen is hence in the circumference region of around 150 μm in width in the tube. Samples for the hydrogen analysis were cut from near the location of those for NIP examinations in the oxidized tubes. The hydrogen concentration was measured by a high temperature extraction method, summarized with sample-ID and the oxidation conditions in Table 1. The sample processed at 973 K contains much higher hydrogen concentration above 1000 wt ppm, the other processed at 1323 K less than 20 wt ppm.

Hydrided Zircaloy-4 tubes with known hydrogen concentrations were prepared by the Nuclear Development Corporation. The hydriding was performed at about 673 K under hydrogen gas flow. The hydrides were uniformly distributed in the tubes. Samples 5 mm in length called the 'standard samples' were cut from those tubes. Hydrogen concentrations in the standard samples were estimated using other samples which were cut from near the location of the standard samples in the hydrided tubes. The concentrations were measured by high temperature extraction method, ranging from around 100 wt ppm to around 2500 wt ppm. The sample-IDs and representative hydrogen concentrations are given in Table 2.

Detailed information about segregated tubes used in the previous work is stated in Ref. [8]. The hydrided area

Table 1
Oxidation conditions and representative hydrogen concentrations for oxidized tubes

Sample ID	Type	Oxidation temperature (K)	Thickness of oxide layer (μm)	Thickness of α-phase layer (μm)	Hydrogen concentration (wt ppm)
Z2OH1	Zircaloy-2	973	30	–	1110
Z2OH2	Zircaloy-2	1323	70	80	13

Table 2
Sample ID and representative hydrogen concentrations for standard samples

Sample ID	Hydrogen (wt ppm)
ZUH-1	88
ZUH-2	501
ZUH-3	955
ZUH-4	1152
ZUH-5	2589

Table 3
Sample ID and representative hydrogen concentrations for segregated tubes

Sample ID	Hydrogen concentration (wt ppm)
ZSH-1	453
ZSH-2	744
ZSH-3	2021
REF.	17

is limited to the outer region of the tube around 0.1 mm in width. The IDs and hydrogen concentrations are given in Table 3. Typical micrographs of cross-section of the oxidized, standard, and segregated tubes are shown in Fig. 1.

Neutron radiography was performed at 2nd Thermal Neutron Radiography Facility (TNRF-2) in JRR-3. TNRF-2 for non-radioactive samples has high performance with providing a high flux neutron beam above 1×10^8 n/cm^2/s and high collimator ratio of 153 [10].

For the imaging plate of NIP method; the BAS-ND-2025 (made by Fuji Film) was used. The samples were fixed with aluminum tape on the cassette installing a piece of NIP. Fig. 2 shows the schematic drawing of arrangement of the examination with 4 s of exposure time. The size of the picture element (pixel) contributing to spatial resolution in the image is around 0.1×0.1 mm^2. A background image, which is an image without samples, was also obtained to confirm incident beam intensity on the samples.

2.2. Image analyses

The images were processed to evaluate hydrogen concentration and distribution using the software 'IP-lab (made by Scanalytics. Inc.)' on a personal computer. Image contrast is determined by the numerical data at each pixel in the image. Image analysis was carried out to investigate the relationship between hydrogen concentration in a sample and values of the photo stimulated luminescence (PSL) in the image. PSL represents the numerical data in a pixel and is proportional to fluence of the neutron beam irradiating on NIP.

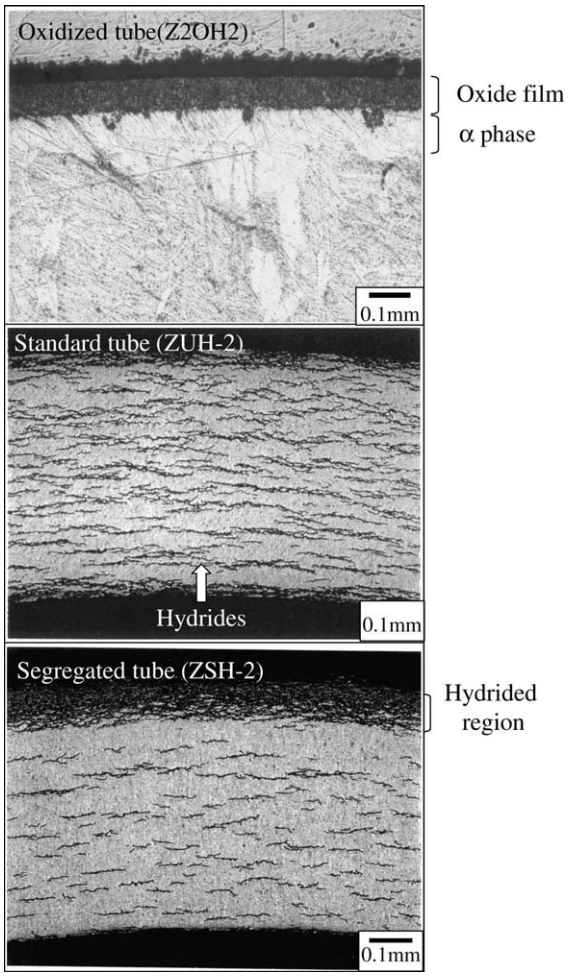

Fig. 1. Typical micrographs of the oxidized, standard, and segregated tubes. All samples were etched by acid to show hydride regions.

The flux of transmitted neutron beam is generally expressed by the following:

$$I_s = I_0 \exp(-\Sigma t), \tag{2}$$

where I_s = transmitted neutron flux [n/cm^2/s], I_0 = initial neutron flux [n/cm^2/s], Σ = macroscopic cross-section of target material [cm^{-1}], and t = transmitted width [cm]. I_s and I_0 can be exchanged for PSL, and Eq. (2) can be rewritten as

$$\frac{\mathrm{PSL}_{\mathrm{image}}}{\mathrm{PSL}_{\mathrm{back}}} = \exp(-\Sigma t). \tag{3}$$

$\mathrm{PSL}_{\mathrm{image}}$ is averaged by PSL on the pixels over the entire image of the sample. $\mathrm{PSL}_{\mathrm{back}}$ is obtained in the background image. It is noted that $\mathrm{PSL}_{\mathrm{image}}$ and $\mathrm{PSL}_{\mathrm{back}}$ are obtained in the same beam-irradiation area to remove the influence of difference in beam intensity in the position. The macroscopic cross-section is expressed as

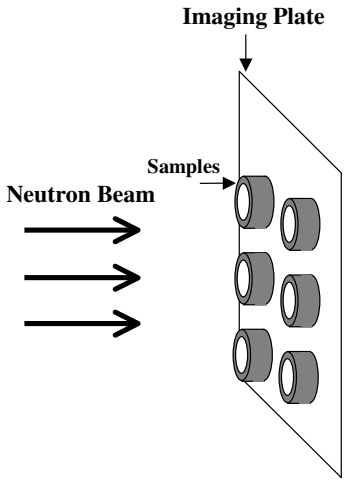

Fig. 2. Schematic drawing of arrangement of NIP method.

$$\Sigma = \sum_i \sigma_i N_i \quad (i = 1, 2, 3, \ldots, m), \tag{4}$$

where σ_i, N_i, and m are microscopic cross-section [cm^2] and number density [atoms/cm^3] of the ith element in an object, and the number of the elements contained, respectively. When elements are added in the Zircaloy, Eq. (3) becomes

$$\frac{\mathrm{PSL_{image}}}{\mathrm{PSL_{back}}} = \exp(-\Sigma_{\mathrm{Zry}} t) \exp\left(- \sum_i \sigma_i N_i t \right) \quad (i = 1, 2, 3, \ldots, m), \tag{5}$$

where Σ_{Zry} is macroscopic cross-section of Zircaloy [cm^{-1}]. Since Σ_{Zry}, σ_i, and t are constants in this work, Eq. (5) shown a relationship between PSL and concentration of added elements.

3. Results and discussion

3.1. Effects of oxide film

Fig. 3 shows the images of the Zircaloy-2 tubes oxidized at 973 and 1323 K i.e., Z2OH1 and Z2OH, respectively. The gray level of Z2OH1 with much hydrogen concentration is obviously different from that of the reference sample. The gray level of image of Z2OH2 is similar to that of the reference tube. The oxide films at the inner and outer sides are not confirmed in either of the images. Z2OH2 with low hydrogen concentration contains the oxide film around 70 μm in thickness and phase around 80 μm in thickness, however, the contribution of oxygen to the image contrast is not recognized. It is hence considered that the difference in the gray level between the reference and Z2OH1 is caused by the hydrides.

Fig. 4 shows profiles of $\mathrm{PSL_{image}}/\mathrm{PSL_{back}}$ on a line in the images of REF., Z2OH1, and Z2OH2 in Fig. 3. There is no appreciable difference between the $\mathrm{PSL_{image}}/\mathrm{PSL_{back}}$ curves of REF. and Z2OH2. It is noted that the hydrogen concentrations in both REF. and Z2OH2 are almost equivalent, below 20 wt ppm. On the other hand, the $\mathrm{PSL_{image}}/\mathrm{PSL_{back}}$ of Z2OH1 with much hydrogen is low in comparison with that of the others.

In these results, it is clarified that the contribution of the oxide film to the images is small. It appears that the contribution of oxygen to gray level in the image can be neglected when hydrogen concentration in irradiated tubes with both hydride and oxide film is estimated by NIP methods. This is a significant result in that the process for hydrogen analysis is simplified.

3.2. Relationship between PSL and hydrogen concentration

Macroscopic cross-section of zirconium atom, length of the tested tube, and microscopic cross-section of a

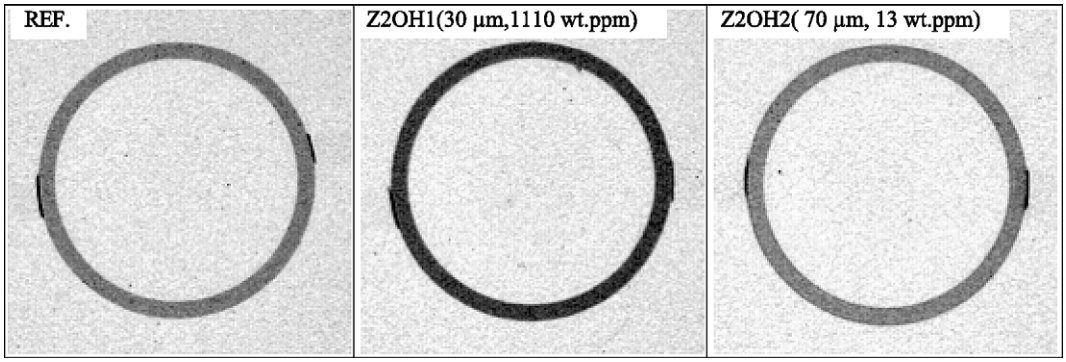

Fig. 3. NIP images of the reference and oxidized Zircaloy-2 tubes. Sample ID, oxide film thickness, and hydrogen concentration are attached in the each image. Because aluminum (Al) tapes contain paste with highly rich hydrogen, gray level in the regions is getting black in comparison with other region.

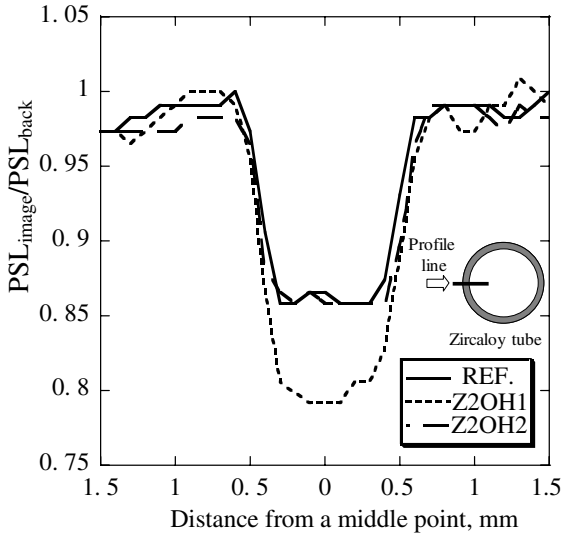

Fig. 4. Profile of PSL_{image}/PSL_{back} in a line in the samples of REF., Z2OH1, and Z2OH2.

hydrogen atom for thermal neutron are around 0.28 cm^{-1}, 5 mm, and around 20.8 barn, respectively [11]. The number density can be transferred to a mass density. The number density and mass density are given in Eqs. (6) and (7), respectively.

$$N_H = \frac{W_H}{W_{Zr} + W_H} \times \rho_{Zr} \div M_H \times A_N \approx \frac{W_H \cdot \rho_{Zr} \cdot A_N}{W_{Zr} \cdot M_H} \quad (W_{Zr} \gg W_H)\ [\text{atoms/cm}^3] \tag{6}$$

$$C_H = \frac{W_H}{W_{Zr} + W_H} \times 10^6 \approx \frac{W_H}{W_{Zr}} \times 10^6 \quad (W_{Zr} \gg W_H)\ [\text{wt ppm}], \tag{7}$$

where N_H = number density of hydrogen in zirconium [atoms/cm^3], C_H = mass density of hydrogen in zirconium [wt ppm], W_H = weight of hydrogen in zirconium [g], W_{Zr} = weight of zirconium [g], ρ_{Zr} = theoretical density of zirconium = (6.52 [g/cm^3]), M_H = mass number of hydrogen = (1.0 [g/mol]), and A_N = Avogadro number = (6.02×10^{23} [mol^{-1}]). Eqs. (6) and (7) hence introduce Eq. (8) as follows:

$$N_H = 3.93 \times 10^{18} \times C_H \quad [\text{atoms/cm}^3]. \tag{8}$$

Eq. (8) changes Eq. (2) as

$$\frac{I_s}{I_0} = \exp(-\Sigma_{Zry} t) \exp(-\sigma_H N_H t) = 0.869 \exp(-4.08 \times 10^{-5} C_H). \tag{9}$$

Taylor expansion about point $C_H = 0$ is performed in the right terms of Eq. (9) in the following:

$$0.869 \exp(-4.08 \times 10^{-5} \times C_H) = 0.869(1 - (4.08 \times 10^{-5} C_H) + (4.08 \times 10^{-5} C_H)^2 \ldots (-1)^m (4.08 \times 10^{-5} C_H)^m) \quad (n = 0, 1, 2, \ldots, m). \tag{10}$$

Due to $(4.08 \times 10^{-5} C_H) \ll 1$ in $C_H < 3000$ wt ppm in the present condition, first approximation can be performed on Eq. (10). Hence, Eq. (10) becomes

$$\frac{I_s}{I_0} = \frac{PSL_{image}}{PSL_{Back}} = 0.869 - 3.55 \times 10^{-5} C_H. \tag{11}$$

3.3. Image analysis for estimation of hydrogen concentration

Fig. 5 shows the images of the standard samples. The degree of gray level in the images is obviously enhanced with increasing the amount of hydrogen concentration. There is almost no gradation of gray level in the images. It is assumed that the absorbed hydrogen is uniformly distributed over the samples. These results show that those are suitable as standard samples.

Fig. 6 shows the relationship between the PSL_{image}/PSL_{back} and hydrogen concentrations in the oxidized and hydrided tubes, and a curve of Eq. (11) is also shown in this figure. Four repetitive tests were performed to investigate the reproducibility. Plotted dots of the standard samples in each test show a linear relationship between the PSL_{image}/PSL_{back} and hydrogen concentrations. The plotted dots of PSL_{image}/PSL_{back} in each test also show reasonable agreement with the linear curve of Eq. (11). However, there is a small shift among the plotted dots of Tests 1–4. The shift of plotted curves indicates that results of NIP method are not compatible among the tests, and unknown samples should be examined with standard samples when NIP method is used for hydrogen analysis. The plotted dot of oxidized sample almost falls on plotted curves of the standard samples. It appears that hydrogen concentration is a governing factor to determine PSL_{image}/PSL_{back} value.

Fig. 7 shows the images and distribution of local hydrogen concentration in the segregated tubes. The images were obtained with standard samples in test 2. An empirical formula is obtained by the plotted data of the standard samples of test 2 in Fig. 6 as:

$$\frac{PSL_{image}}{PSL_{back}} = 0.877 - 4.43 \times 10^{-5} C_H, \tag{12}$$

where C_H = hydrogen concentration [wt ppm]. Eq. (12) shows the relationship between the hydrogen concentration and PSL_{image}/PSL_{back}. The concentrations in local areas are introduced by substituting PSL_{image}/PSL_{back} at pixels in the image in Eq. (12). Fig. 8 shows the relationship between average hydrogen concentration over

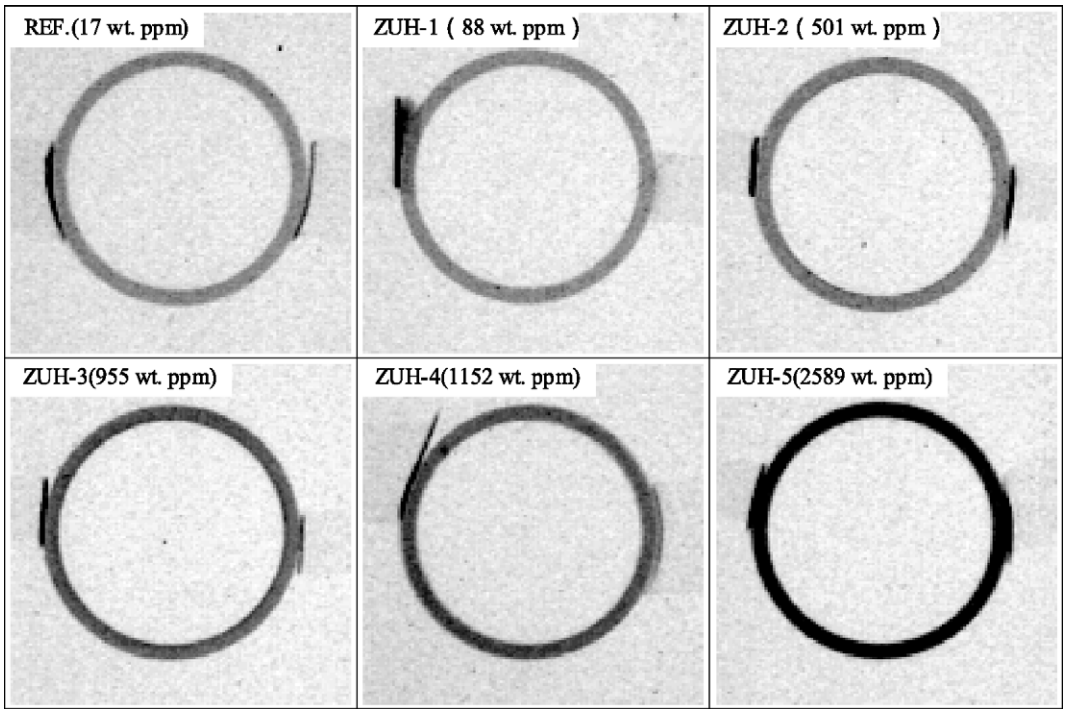

Fig. 5. NIP images of the standard tubes with the reference tube.

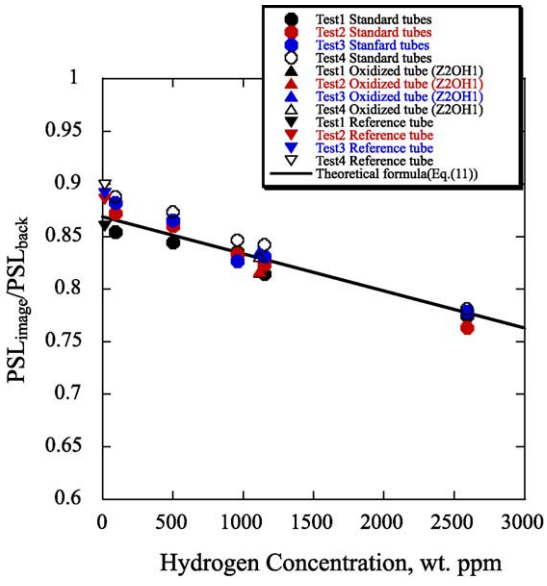

Fig. 6. Relationship between PSL_{image}/PSL_{back} and hydrogen concentration on the standard and oxidized tubes. In addition, a curve of theoretical formula (Eq. (11)) is shown.

the sample and local hydrogen concentration in hydrided region [12]. Average hydrogen concentration of ZSH1 and ZSH2 are 453 and 744 wt ppm, respectively. The local concentration at the hydrided region in ZSH1 and ZSH2 reasonably corresponds to that of the literature data. The hydrogen concentration of the hydrided region in ZSH3 is 2021 wt ppm and cannot be estimated by the literature data because of being too large in value.

In the case of high temperature extraction method, the hydrogen concentration in only one sample is measured in a single examination. On the other hand, NIP method can measure hydrogen concentrations in several samples in one examination. The examination is simple and non-destructive. The distribution of hydrogen concentrations over the cross-section of the samples can be obtained, although being integrated along the neutron beam direction. In addition, standard samples with known hydrogen concentrations are required to determine the hydrogen concentration of unknown samples. Information about correct hydrogen concentrations in the standard samples is hence required. Moreover, the accuracy of hydrogen analysis by NIP method is not adequate. The range of numerical data in the image reader used in this work is from 0 to 1023 i.e., 10 bits. Difference in the averaged numerical data between the images of REF with 17 wt ppm H and ZUH-5 with 2589 wt ppm H is only 16. It is noted that the amount of concentration of absorbed hydrogen into a Zircaloy tube in PWR is at maximum 500 wt ppm around 50 GWd/t in the extended burn-up [13]. Probably, the accuracy of NIP method is not enough yet, in estimating

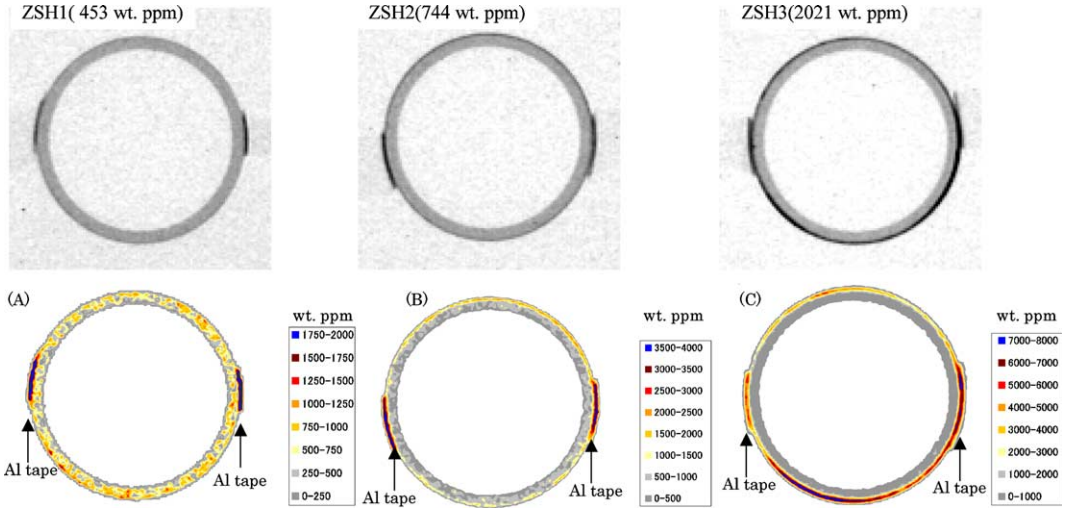

Fig. 7. NIP images and maps of local hydrogen distribution in segregated tubes are shown. The map (A), (B), and (C) correspond to images of ZSH1, ZSH2, and ZSH3. It is noted that color scales in each map are different.

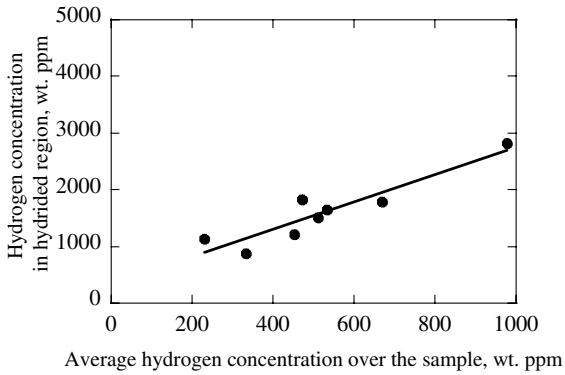

Fig. 8. Relationship between the average hydrogen concentration in the hydrided region and entire sample in the segregated samples [12].

the hydrogen concentration in the practical samples. In addition, since NIP has sensitivity to gamma rays, it is necessary to take into account the effect of gamma rays emitted from activated samples on NIP images. An image reader and NIP itself with good performance is hence required to achieve more accurate evaluation of the hydrogen concentration in irradiated cladding tubes by NIP method.

4. Summary

A linear relationship between hydrogen concentration and PSL_{image}/PSL_{back} in standard samples is obtained. The plotted curves of hydrogen concentration – PSL_{image}/PSL_{back} are in reasonable agreement with a theoretical formula. Distribution of the local hydrogen concentration in segregated tubes is obtained by using the standard samples. The size of the localized area is small, 0.1×0.1 mm^2 equivalent to a picture element in NIP image. It is clarified that there is no contribution of oxide film in the tubes to NIP image contrast. This result is significant in that the influence of the oxide film can be ignored in hydrogen analysis by NIP method.

Acknowledgements

The authors are grateful to Dr T. Kodaira, Messrs M. Shindo, F. Kanaizuka, Y. Nishino, and Dr F. Nagase for valuable advice and useful discussions. The authors are indebted to Mr H. Andou and staff of JRR-3 for technical support in the examinations and are also grateful to Messrs T. Otomo, I. Takahashi, Y. Nihei, and staff of Reactor Fuel Examination Facility for support in sample fabrication and measuring hydrogen concentrations.

References

[1] S.-Q. Shi, G.K. Shek, M.P. Puls, J. Nucl. Mater. 218 (1995) 189.
[2] G. Meyer, M. Kobrinsky, J.P. Abriata, J.C. Bolcich, J. Nucl. Mater. 229 (1996) 48.
[3] F. Garzarolli, H. Seidai, R. Tricot, J.P. Gros, ASTM STP 1132, Zirconium in the Nuclear Industry, 1991, p. 395.
[4] P. Von Der Hardt, H. Rottger (Eds.), Neutron Radiography Handbook (Nuclear Science and Development), D. Reidel Publishing Company, Dordrecht, Holland, 1981, p. 58.

[5] J.P. Barton (Ed), Neutron Radiography, Proceedings of the first WCNR, 1983, p. 437.
[6] H.H. Klepfer, H.D. Kosanke, E.L. Esch., ASTM STP 458, Applications Related Phenomena in Zirconium and its Alloy, 1969, p. 372.
[7] N. Niimura, Y. Karasawa, I. Tanaka, J. Miyahara, K. Takahashi, H. Saito, S. Koizumi, M. Hidaka, Nucl. Instrum. and Meth. A 349 (1994) 521.
[8] R. Yasuda, M. Matsubayashi, M. Nakata, K. Harada, J. Nucl. Mater. 302 (2002) 156.
[9] B351-85, in: R.A. Storer, J.L. Cornillot, P.C. Fazio, M. Gorman, E.L. Gutman, C.T. Hsia, G. Johns, J. Kramer, C.M. Leinweber, P.A. McGee, S.P. Milligan, K.W. O'Brien (Eds.), Annual Book of ASTM Standards Vol. 02.04, 1990, p. 157.
[10] M. Matsubayashi, H. Kobayashi, T. Hibiki, K. Mishima, Nucl. Technol. 132 (2000) 309.
[11] Data of JENDL – 3.2, <http://wwwndc.tokai.jaeri.go.jp/jendl/j32/j32.html>.
[12] F. Nagase, T. Otomo, H. Uetsuka, Japan Atomic Energy Research Institute Reports, JAERI-Research 2000 46 December 2000 (in Japanese).
[13] D. Deydier, in: IAEA Technical Committee Meeting, Rez near Prague, The Czech Republic, October, 1993.